Materials and Structures (2024) 57:88
https://doi.org/10.1617/s11527-024-02370-6

ORIGINAL ARTICLE

Recycling of incinerated sewage sludge ash and waste glass powder in alkali-activated slag for sewer rehabilitation

Keke Sun · Hafiz Asad Ali · Yamei Cai · Dongxing Xuan · Chi Sun Poon

Received: 20 January 2024 / Accepted: 17 April 2024

Abstract A new era has dawned in the manufacturing of cement-free binders with appropriate mechanical strengths and durability to combat CO_2 emissions. However, the assessment of their performance in extreme conditions is ongoing. Here, we attempted to use incinerated sewage sludge ash (ISSA), a waste product of sewage sludge incineration that contains limited amounts of heavy metals, along with waste glass powder (GP) and ground granulated blast furnace slag (GGBS), as precursors to produce cement-free binders through alkali-activation. The alkali-activated materials (AAMs) were then subjected to an intensified sewage corrosion test for 6 months. The aim was to utilize the heavy metals in the ISSA as biocides to resist the biogenic acid attack on the AAMs. The experimental results indicated that superior performance was achieved by using a ternary binder prepared with ISSA, GP, and GGBS under biogenic acid simulation. Such enhanced durability can be attributed to the low Ca content in the resulting alkali-activated gels, which also reduced the grain size of gypsum formed and prevented expansion deterioration. Furthermore, the slow release of heavy metals from the AAMs prepared with the ISSA, evidenced by the leaching test results, was able to inhibit microbial growth.

Keywords Alkali-activated materials · Waste glass · Incinerated sewage sludge ash · Leaching · Biogenic acid attack

1 Introduction

Poor durability of ordinary Portland cement (OPC) in sewage environments is frequently reported which is mainly caused by physical, chemical, and microbial processes (collectively called microbial-induced concrete corrosion (MICC)), happening in wastewater systems [1, 2]. During long-term exposure, MICC are caused by sulfur-related bacteria, especially sulfur-oxidizing bacteria (SOB) and sulfate-reducing bacteria (SRB) [3, 4]. The formation of aqueous hydrogen sulfide $H_2S_{(aq)}$ may be considered the starting point for the MICC in the sewerage systems. These microorganisms can utilize the diffused $H_2S_{(aq)}$ as a food source and oxidize sulfur compounds to sulfuric acid. Due to their alkaline nature, cement-based materials are susceptible to degradation when exposed to acidic conditions. The in-situ production of sulfuric

Supplementary Information The online version contains supplementary material available at https://doi.org/10.1617/s11527-024-02370-6.

K. Sun · H. A. Ali (✉) · Y. Cai · D. Xuan · C. S. Poon (✉)
Department of Civil and Environmental Engineering and Research Centre for Resources Engineering Towards Carbon Neutrality, The Hong Kong Polytechnic University, Hung Hom, Kowloon, Hong Kong, China
e-mail: hafiz-asad.ali@polyu.edu.hk

C. S. Poon
e-mail: cecspoon@polyu.edu.hk

Published online: 02 May 2024

acid leads not only to the etching and corrosion of concrete surfaces but also the formation of expansive gypsum and ettringite at the expense of calcium hydroxide and tricalcium aluminate [5–7]. Therefore, this MICC deteriorates the physicochemical properties of concrete (e.g., cracking, spalling, and strength loss), shortens the service life, and even may cause catastrophic structural failures.

Various strategies have been employed to reduce the risk of damage caused by concrete bio-corrosion, such as improving concrete design features, controlling the sewer environment, and applying chemicals or antimicrobial coatings [8–11]. Among them, modifications of concrete mixes and applications of antimicrobial coatings on the surface of concrete are two effective methods to prevent bio-corrosion. Generally, the impermeability and acid resistance of concrete can be improved by the incorporation of supplementary cementitious materials (e.g., slag, silica fume), and the use of calcium aluminate cement has also been found useful. Moreover, some coatings prepared with inorganic or organic cementitious material as the matrix, and bactericide as functional components have exhibited antibacterial or bactericidal capability. But the long-term durability of these materials in the corrosive sewerage environment is still a major problem. Compared to OPC, using alkali-activated materials (AAMs) can enhance the acid resistance due to the lower amounts of Ca in the reaction products, which prevents the decalcification and dealumination of the gel phases [12–14]. However, the traditional AAMs lack a bactericidal ability that prevents the growth of the acid-producing bacteria on their surfaces. One strategy that can be adopted is to incorporate biocides (e.g. Al, Fe, Cu, Ag, and Zn-containing compounds or organic, oxidizing, or non-oxidizing compounds) in the concrete or the coating materials that may inhibit the growth of microbes [5, 15]. The treatment aims to control or inhibit the activities of microorganisms, e.g. SRB and SOB, to a sufficiently low level. To maintain long-term effects, it is a normal practice to apply biocide treatments periodically. Despite their proven efficiency, the undesirable leaching of the biocides to the sewage, as well as their short bio-resistance lifetime, necessitates the search for more efficient, environmentally friendly, and long-lasting alternatives. Moreover, one concern with the use of biocides is the potential environmental impact, as many of them are toxic.

AAMs are usually produced by the polymerization of aluminosilicate precursors such as coal fly ash, metakaolin, and granulated ground blast furnace slag (GGBS) by alkali activators [16–18]. The aluminosilicate precursors derived from local waste streams can be used as environmentally-friendly alternate precursors to address the cost and availability limitations. For example, in Hong Kong, waste glass contributes to a significant proportion of municipal solid waste (290 tonnes/day), and only about 20% of waste glass is recycled due to the lack of a local glass manufacturing industry [19]. As a potential alkali-siliceous material, waste glass powder (GP) has been investigated extensively as a precursor to producing AAMs [20]. Moreover, in Hong Kong, approximately 1200 tonnes of sewage sludge are produced daily, and the largest sewage sludge incinerator in the world (with a capacity of 2000 tonnes/day) has been constructed, which can reduce the sludge mass by almost 90% [21]. But there are still about 120 tonnes/day of the incineration sewage sludge ash (ISSA) required to be disposed of at landfills. Though the leaching risk of heavy metals from the ISSA is relatively low because of the stringent control of industrial effluent, landfill disposal is inadvisable because of their limited landfill capacity in Hong Kong, and the wasting of recoverable resources [22]. In previous studies [23–25], appropriate reuse and resource recovery options for the ISSA and waste glass were proposed to prepare AAMs. However, their long-term durability in the corrosive sewerage environment still needs to be addressed.

The study explored the feasibility of using (i) incinerated sewage sludge ash (ISSA), which not only contains aluminosilicates as the precursor but also contains certain amounts of heavy metals (e.g. zinc and copper) as a source of bactericidal agent, (ii) waste GP as it contains a considerable amount of amorphous silica which can react with the alkali in the geopolymerization process and reduce the amount of acid dissolvable Ca-gels along with traditional precursor, i.e. GGBS in formulating AAMs that can resist sewage corrosion effectively. To verify the hypothesis, a laboratory simulated sewage corrosion experiment was conducted. In this study, the compressive and flexural strength of the AAMs after exposure to the aggressive sewage environment were evaluated, and the microscopic characteristics were examined by using SEM–EDS and XRD. Combined with the leaching study results, the improvement

effect of the ISSA on the sewage corrosion for AAMs was revealed. This study aims to utilize two local solid wastes (e.g., ISSA and GP) for the development of novel microbial-resistant AAMs for sewerage infrastructure rehabilitation.

2 Materials and methods

2.1 Precursors and activators

Soda-lime waste glass powder (GP), granulated ground blast furnace slag (GGBS), and incinerated sewage sludge ash (ISSA) were used as precursors for designing one-part alkali-activated materials (AAMs) mortars. An industrial-grade Na_2SiO_3-anhydrous powder comprising 35.8% SiO_2 and 62.9% Na_2O by weight was used as the alkali activator. The soda-lime waste glass cullet was collected from a local recycler in Hong Kong, and the cullet was ground for 4 h using a laboratory ball mill to produce the glass powder. Prior to grinding, mixed colored glass cullet (i.e., green, brown, white, blue glass cullet), were washed with tap water to remove contaminants, followed by drying for 24 h at 105℃. The ISSA was obtained from the sewage incineration facility (T park) in Hong Kong, and the GGBS was supplied by a commercial supplier in China. The chemical compositions of the GGBS, GP, and ISSA are determined via the X-ray fluorescence analysis (Rigaku Supermini 200 spectrometer), and the results are presented in Table 1. The ISSA mainly consisted of SiO_2, Al_2O_3 and Fe_2O_3, and small amount of CaO, showing compositional resemblance to coal fly ash, and traces of heavy metals (e.g., ZnO, CuO and PbO) were also present [22]. Moreover, the ISSA has a higher loss on ignition (LOI) than GP due to the presence of unburned organic compounds and moisture. The negative LOI values of GGBS meant a gain of weight after ignition, which may be due to the oxidation of the sulfide during ignition [26]. Figure 1a shows the particle size distribution of GGBS, GB and ISSA, which was obtained by a laser diffraction analyser (Malvern Mastersizer 3000E). Regarding the particle size distribution, the GP, GGBS and ISSA exhibited D_{50} of 27 μm, 12 μm, and 13 μm, respectively, meaning

Table 1 Chemical compositions of GP, GGBS, and ISSA (wt%)

	Na_2O	MgO	Al_2O_3	SiO_2	P_2O_5	SO_3	CaO	TiO_2	Cr_2O_3	Fe_2O_3	CuO	ZnO	PbO	Others	LOI
GP	13.17	1.64	2.1	67.89	0.1	0.14	10.8	0.1	0.2	–	–	–	0.03	3.86	0.79
GGBS	–	7.32	14.22	34.78	–	3.12	38.38	0.71	–	0.27	–	–	–	0.77	−0.32
ISSA	3.43	2.17	12.9	49.5	8.72	1.7	6.35	0.44	0.06	12.6	0.079	0.24	0.008	1.80	4.48

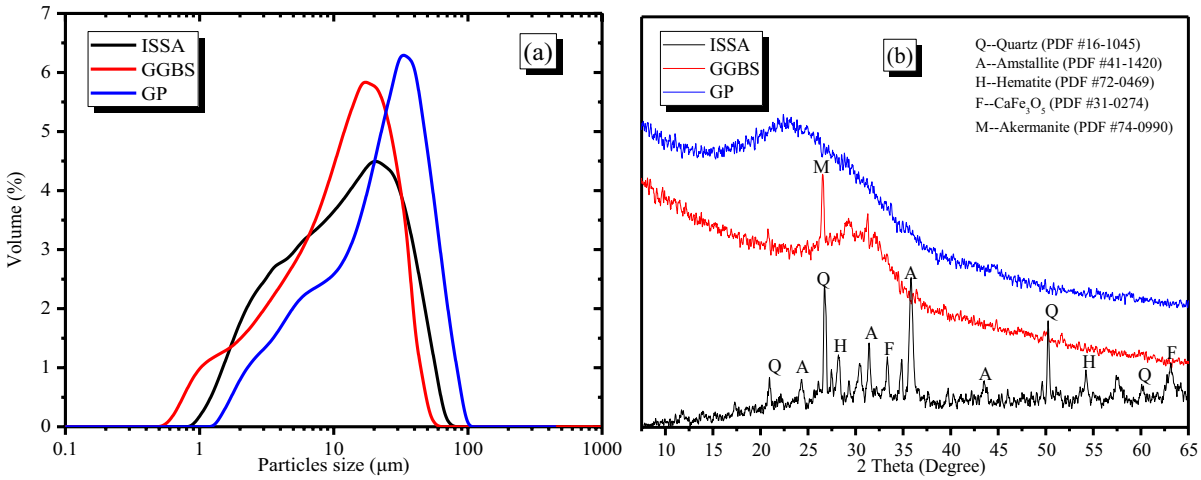

Fig. 1 Particle size distributions and XRD patterns of raw materials

that GP was relatively coarser than ISSA and GGBS. According to the XRD patterns, the GGBS and GP showed a broad, amorphous hump with no distinct crystalline peaks. Still, the ISSA exhibited many crystalline phases indicating the presence of quartz, whitlockite and some iron compounds. In addition, the rive sand with a particle size less than 1.18 mm was chosen as the fine aggregate.

2.2 Sample preparation

The simplex-centroid design method and a ternary contour diagram were used to obtain the optimized composition or compositional range for the alkali-activated ternary composites [24]. The mix proportions of the one-part AAM mortar are listed in Table 2. Firstly, the proportioned precursors, activator and rive sand were dry mixed for 3 min using a laboratory mixer. Then, the mixing water was added for another 3 min. The mortar specimens were cast into 40 mm × 40 mm × 160 mm molds, vibrated for 1 min to remove air bubbles and covered with plastic sheets to avoid moisture loss. Moreover, the AAM pastes (without aggregate) were prepared using the same water/precursor ratio, and then cast into 40 mm × 40 mm × 40 mm molds for the microstructure and leaching tests. After 24 h, all AAM mortar and paste specimens were demolded and transferred into a curing room (25 °C and RH = 95%) for 28 days. After 28 days, the AAM pastes and mortars were transferred to the water and sewage solution, and the water-cured samples were taken as the reference sample to calculate the strength loss. Moreover, the SEM and XRD analyses were carried out for the microstructural changes of AAM paste.

2.3 Experimental methods

2.3.1 Sewage corrosion of AAMs mortar and paste

Figure 2 depicts the simulated sewage corrosion device. The simulation chambers provided an environment to simulate the degradation process of the AAM mortar/paste subjected to a real sewer environment. 20 kg of nutrient solution and 1 kg of activated sludge collected from a local sewage treatment work were used. The AAM specimens were placed on a plastic grid, and semi-submerged into the solution fully and evenly for 6 months. The activated sludge collected from a local sewage treatment work was poured into the chamber, while a nutrient solution containing deionized water and auxiliary chemicals as nutrients (200.0 g starch, 110.0 g glucose, 28.5 g peptone, 12.0 g urea, 6.7 g $(NH_4)_2HPO_4$, 3.6 g $MgSO_4$, 1.2 g NaCl) were also added [8, 27, 28]. In addition, the sulfate-reducing bacteria (SRB) grow optimally within 20 ~ 35 °C dictated by the ability of proteins within the cell to function [29]. Therefore, a constant temperature (28–30 °C) environment was provided by a stainless-steel heater to ensure the growth of the microorganisms, and a mixer with 800 rpm was fixed to the simulation chambers to provide continuous agitation and prevent the materials from settling. One-third of the solution was replaced with the fresh nutrient solution every 7 days. The pH value of sewage was measured by a Mettler Toledo pH meter, and

Table 2 Mix proportions of the ternary AAMs mortars

	Precursor (wt%)			Activator/precursor ratio	Aggregate/precursor ratio	Water/precursor ratio
	GGBS	GP	ISSA			
1	0	100	0	0.15	1	0.4
2	50	50	0			
3	100	0	0			
4	50	0	50			
5	0	0	100			
6	0	50	50			
7	50	25	25			
8	25	25	50			
9	25	50	25			
10	75	12.5	12.5			

Fig. 2 Photo of sewage corrosion device

the chemical oxygen demand concentrations (COD) were determined according to the APHA, 2012 measured during the sewage corrosion test [30].

2.3.2 *Physical properties*

In previous studies [31, 32], the formation and composition of biofilm was very sensitive to the temperature. To reduce the effect of temperature on the biofilms, the AAMs samples after the sewage corrosion test, were air-dried for 48 h, and then signs of cracking and physical changes on the specimens were visually observed and photographed. The flexural and compressive strengths of the AAMs mortar were measured by a compression machine following BS EN 12390-5. The water-cured AAMs mortar was used as a control sample, and the loss ratio of the flexural and compressive strengths of the AAM mortars after sewage erosion was calculated. During the sewage corrosion, the alkaline solution in the AAMs can be first neutralized by the diffusion of the biological sulfuric acid, then the structure and properties deteriorated. The deterioration process was usually accompanied by a decrease in pH value of the pore solution from the core to the surface of the AAMs sample. Therefore, after the flexural strength test, the broken specimens were sprayed with a 1% phenolphthalein solution indicator to assess the pH change along the cross-section of each AAM mortar. Furthermore, the mass loss of the AAM mortars after removing the loose and deteriorated mass was calculated. The average value of six replicates was taken as the representative value.

2.3.3 *Leaching of heavy metals*

Due to stringent environmental regulations about the safe and controlled release of heavy metals into the environment, the ASTM C1308 was conducted on the AAMs for evaluating the leaching of heavy metals from the mixtures. The AAMs specimen with the size of 40 mm × 40 mm × 40 mm was fully soaked in 1200 mL Milli-Q water. After every week, the leachant was changed, and its concentration was tested using an inductively coupled plasma/optical emission spectroscopy (ICP-OES, FMX36, SPECTROBLUE). The cumulative fraction of heavy metals was calculated by the sum of the fractions of a species leached during all sampling intervals. The test was conducted at a temperature of 20 ± 1 °C.

2.3.4 *Microstructural analysis of hardened AAMs*

The AAM pastes after the sewage corrosion test were crushed into small fragments, followed by stopping the alkali activation reaction with solvent (ethyl alcohol)-exchange method for a week. The SEM–EDX analysis of the eroded surface and polished cross-sections of the carbon-coated paste fragments was recorded using a Tescan Vega 3 scanning electron microscope equipped with energy-dispersive X-ray spectroscopy under high vacuum conditions with 20 kV of beam intensity. In addition, X-ray diffractometry (XRD, Rigaku Smart Lab-Advance) was used to characterize the crystalline phases of the powdered samples obtained from the AAM paste fragments. The scan range, step size, and dwelling time of

the XRD test were 5–70°, 0.02° and 1*s*, respectively. Before the microstructural analysis tests, these fragments were dried at 40 °C in a vacuum oven for a week to preserve their structure as closely as possible to their natural state [23].

3 Results

3.1 Characteristics of artificially intensified sewage

The COD content in the sewage is a critical factor for sulphide buildup and its subsequent release into the surrounding air. The COD and pH values of the artificially intensified sewage were recorded periodically for 90 days. The results are shown in Fig. 3. A considerable variation in COD with time was observed. The COD of the artificially intensified sewage was more than 18,000 mg/L, 300 times the concentration in ordinary sewage, indicating the well-accelerating setup for the sewage corrosion test [33, 34]. This high COD indicated a greater amount of oxidizable organics in the artificially intensified sewage that helped reduce the dissolved oxygen and induced an anaerobic environment in the chamber. Moreover, the initial pH value of the sewage in the chamber was about 8.2. Before 7 days, the pH value of the sewage showed a decrease to about 4.2, followed by an increase to about 5.6. The dramatic reduction of the pH value in the initial sewage was due to the formation of sulfuric acid. It had been reported that when the pH value was lowered to ~9, the microbial communities (e.g. SOB) would develop and oxidize $H_2S(g)$ to sulfuric acid in the presence of sufficient moisture, nutrients, and oxygen [35]. The rise in pH value from 4.2 to 5.6 was attributed to the diffusion of alkali ions from the AAMs' pore solution, which helped neutralize the sulfuric acid. After 7 days, the pH dropped to around 5.2, meaning a formation of a weak acid environment in the chamber due to chemical and biological processes. The reason for the weak acid environment might be related to the higher metabolic rate of the SOB than the diffusion rate of alkali ions. The stabilization of the weak acid environment after 7 days could be achieved, indicating that the formation of acid and diffusion of alkali ions in the sewage solution was in a dynamic equilibrium. Theoretically, the COD would increase with the age, and the pH value of the sewage solution would be decreased due to the presence of sulfuric acid produced by microbial metabolism. However, it can be seen from Fig. 3 that the pH values of the sewage remained stable despite the increase in the COD. The most possible reason might be result from the microbial competition of the SRB and SOB. The metabolic rate of the SOB in the sewage was restrained to a certain extent and caused a

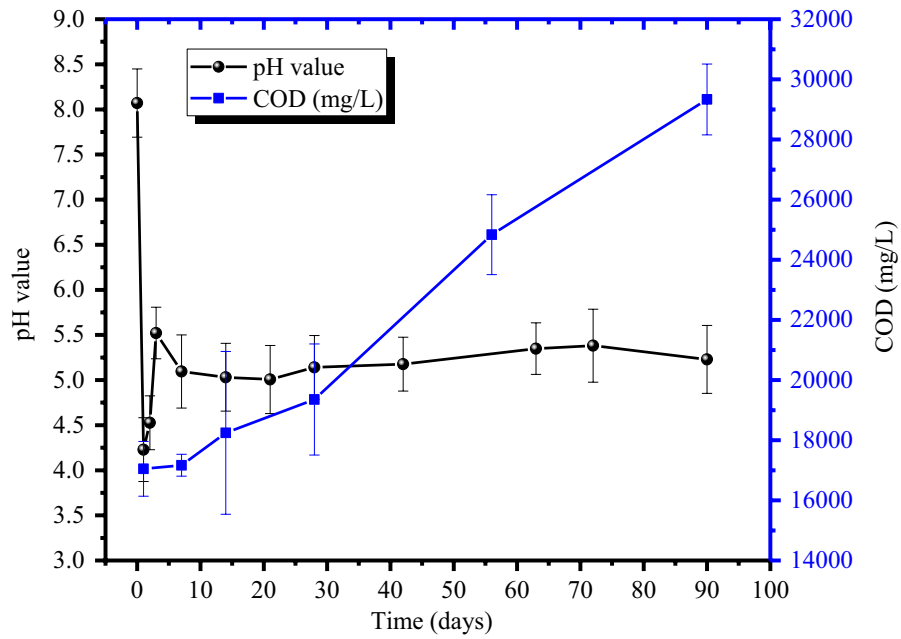

Fig. 3 Chemical oxygen demand (COD) and pH of artificially intensified sewage

stable formation of acid, which would be further verified in the future.

3.2 Visual observation of AAM mortars after the sewage corrosion test

The appearance of the AAMs samples before sewage corrosion was depicted in Fig. S1. After the sewage corrosion test for 6 months, the physical changes, cracks or damages that appeared on the surfaces of AAM mortars were visually assessed, as shown in Fig. 4. No significant signs of deterioration or cracking were observed in the AAM mortars in the submerged region, while color changes and minor cracking were mainly observed in the splashing and non-submerged regions. For example, sample 1 (100% GP) showed minor surface cracking at the splashing region. The reason could be due to the intrinsic behavior of the alkali silica gels produced from alkali-activated GP under wetting–drying

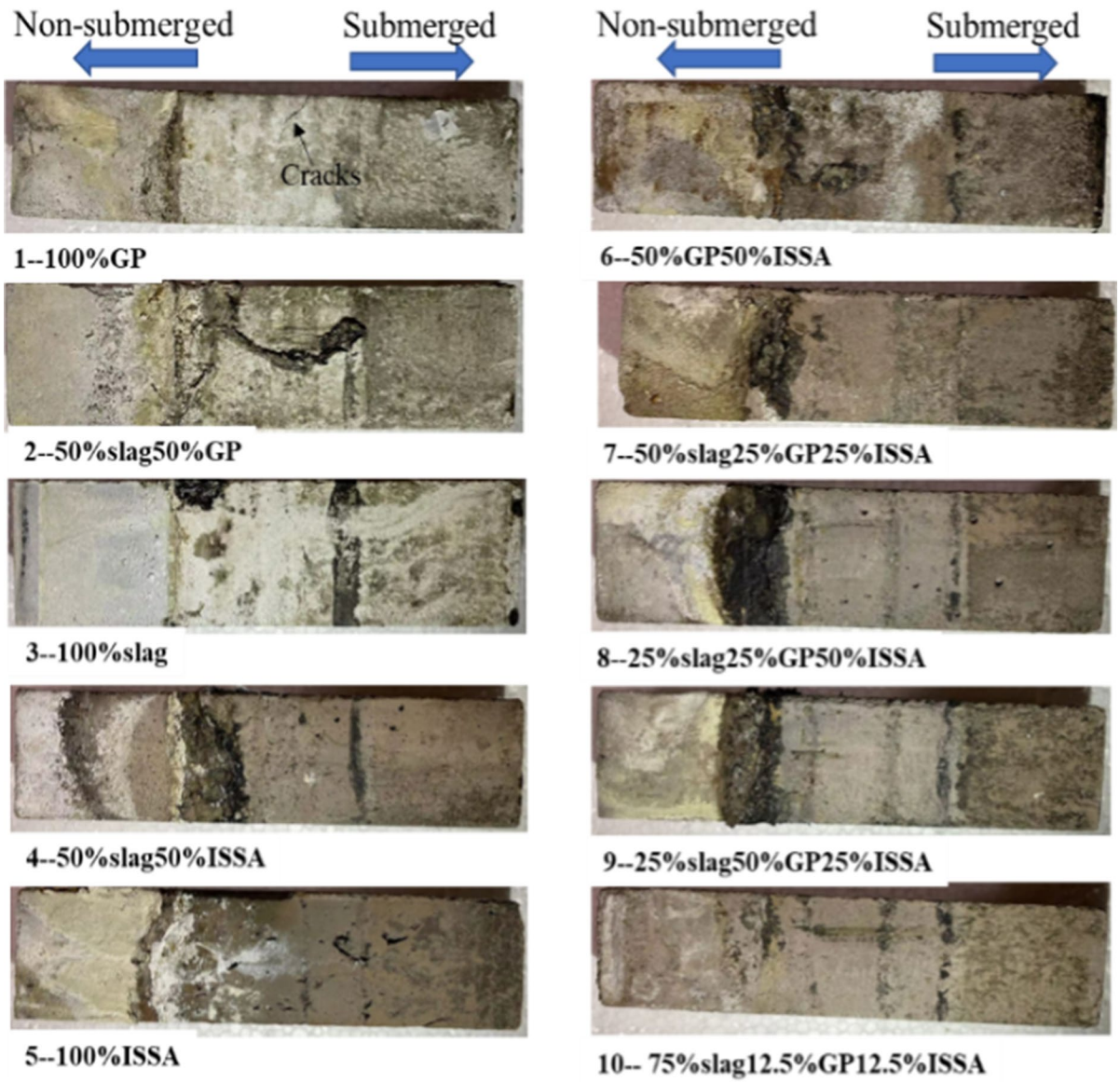

Fig. 4 Surface morphologies of the AAMs after sewage corrosion test

cycles. Similarly, the alkali-activated GGBS and/or GP composites (e.g., samples 1, 2 and 3) showed some signs of deterioration in the non-submerged region, and slight color changes were seen after the biogenic activity. On the other hand, the incorporation of the ISSA into the AAMs showed a color change from initially brownish (before the attack) to white or a light yellowish color (after the attack), mainly in the non-submerged region. The whitish deposits that appeared on these samples' surface resulted from efflorescence formation due to the residual alkali ions leaching from their AAMs matrices. This color change might be attributed to the heavy metal from the ISSA (e.g., Cu, Zn and Fe) interactions with the acidic environment, leading to the precipitation of small amounts of deposits (e.g., the CuS, FeS and $FeSO_4$) at the acidic conditions [3, 36]. Furthermore, various deposits with a light yellowish color were visible and gathered on the non-submerged surfaces of the AAMs, indicating the formation of biofilm by microbial metabolism. The light yellowish biofilm might be attributed to the occurrence of sulfur, indicating the simultaneous H_2S production and oxidation [34]. Besides, some black-colored biofilms (slime layers) at the air-sewage interface were also observed due to melanin that was metabolized by microorganisms in the sewage, and the formation of the biofilm was due to the transfer of oxygen or other chemicals involved in microbial metabolism and the surface of the AAMs. However, the amount of biofilm (or slime layer) in sample 10 (75% GGBS, 12.5% GP and 12.5% ISSA) was visually the least among all the AAMs specimens. This meant that a low substitution level of ISSA and GP (collectively 25 wt% of the total binder) in the AAMs effectively controlled the microbial growth. The bacteriostatic effect of this binder might be linked to the presence of heavy metals in the ISSA that released and controlled the biofilm formation. Another interesting finding was that excessive ISSA dosages resulted in higher amounts of biofilm formation on the AAMs surface. This behavior might be ascribed to that the leaching of the amphoteric heavy metals (e.g., Zn, Cu, Co and Pb) from the ISSA was dependent on the acid–base property of the solution. The low reactivity of ISSA in the AAMs resulted in a high amount of unreacted activator which increased the pH of the pore solution. The heavy metal in the high alkali solution would tend to form insoluble or slightly soluble salts, which decreased the heavy metals leaching.

The loss of alkalinity from the AAMs after the sewage corrosion test was analyzed by spraying 1% phenolphthalein indicator on the freshly broken surfaces. After the biogenic attack, three different zones of the AAMs can be noticed, including the core region of the non-corroded zone, neutralization zone, and corroded zone, depending on the color and physical changes in the AAM matrices. From Fig. 5, the pink-colored area corresponded to the intact (non-corroded) region, meaning that the material still had a high pH environment. In contrast, the whitish or brownish colored area (similar to the original color of the AAM mortars), corresponded to the neutralization zone of the specimens. Due to the presence of the surface porosity of AAMs, the bacteria (e.g. SOB) could penetrate the deeper layer through the pores to produce the biogenic sulfuric acid, reducing the pH value of the pore solution. Therefore, the formation of the neutralization depths might be linked to the unreacted residual alkali and released alkali from the gel matrix, which was then neutralized by the diffusion of biogenic acid [37, 38]. The ISSA-rich AAM mortars showed almost complete loss of alkalinity (viz. samples 5, 6 and 8), followed by the GP-rich mixtures. This behavior was due to the higher alkalis leaching from these mixtures because of the slower reaction rates of ISSA and GP in alkaline media. Moreover, the higher reactivity of GP than ISSA contributed to the formation of more gel and a dense microstructure, thereby preventing alkali leaching from the GP-rich mixtures. Therefore, the GP-rich mixtures showed a lower alkalinity loss than the ISSA-rich mixtures. Although the ISSA-rich mixtures (samples 4, 5, 6 and 8) almost lost all their alkalinity (no pink color of the phenolphthalein indicator was observed), there were no clear corroded regions. The results illustrated incorporation of the ISSA could lead to an acceleration effect on the neutralization of residual alkali, but the effect of the biogenic acid or microbe on the corrosion rate of the AAMs was limited. On the other hand, the mixtures with higher amounts of GGBS densified the matrices and limited the alkalinity loss. Specimens 2, 3, 7 and 10 behaved similarly and contained three clear zones, namely, the outermost 2–3 cm of heavily corroded zone, neutralization zone, and non-corroded zone

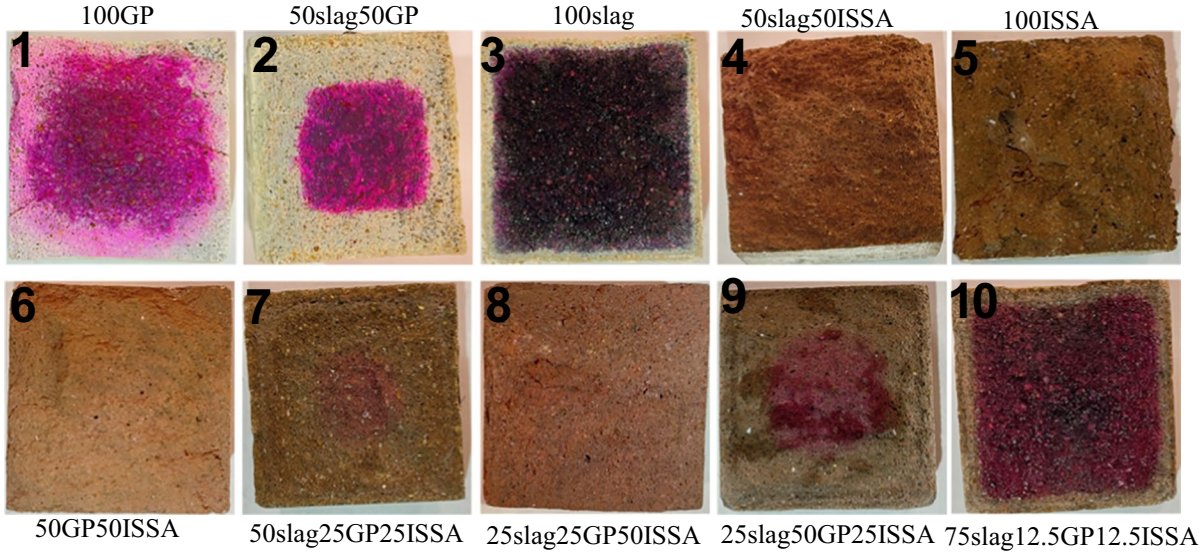

Fig. 5 Cross-section morphologies of the AAMs after the sewage corrosion measured by spraying 1% phenolphthalein indicator

(as shown in Fig. S2). The formation of the heavily corroded zone was closely related to the decalcification of C–A–S–H/N(–C)–A–S–H gel, resulting in the formation of expansive gypsum. This will be further explored in the mineralogical and microstructural evolution sections. Overall, the results suggested that using small dosages of ISSA and GP in the alkali-activated materials, the biogenic resistivity of the ISSA- and GP-AAM mixtures performed similarly to the GGBS alone-based AAMs.

3.3 Change in mass after sewage corrosion test

Figure 6 shows the change in mass of the AAM mortars after exposure to the aggressive sewage environment. All AAM specimens showed some mass losses, although no disintegration of the structure (as shown in Fig. 4) was observed. Therefore, it can be inferred that the mass loss might be attributed to the leaching of the unreacted alkalis, and the dealumination and decalcification/desodiumization of the C–(N)–A–S–H and N–A–S–H gels. The AAMs prepared with a high GGBS (> 65 wt. %), low GP (< 20 wt%) and ISSA (< 15 wt%) contents showed lower mass loss values (below 3.3%), which could be attributed to the higher amounts of stable reaction gels. In addition, the lower mass loss (less than 5 wt%) of the GP/GGBS-rich AAMs was associated

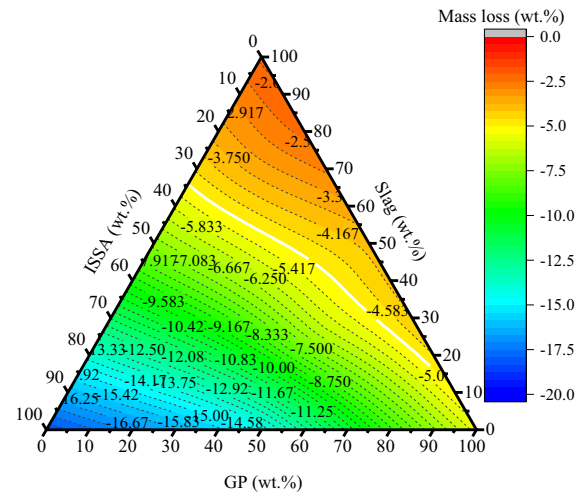

Fig. 6 Change in mass of the AAM mortars after the sewage corrosion test

with the amount of biofilm growth. To some extent, the biofilm formation located on the AAMs mortar surface would provide a protective barrier reducing the transmission of corrosive substances into the sewage [35, 39]. On the other hand, the mass loss of AAMs increased with the increase of the ISSA content, and the maximum mass loss (about 17.8%) was found in the sample prepared with 100% ISSA. This could be related to the instability of reaction products,

meaning that these gels could be easily decomposed (insufficient calcium or aluminium contents) when exposed to aggressive environments. Moreover, the slow reactive ISSA also allowed a large amount of unreacted alkalis and hydroxyl ions to leach out from the pore solution, thus resulting in the formation of efflorescence. It is worth noting that efflorescence formation is the quick and dominant degrading phenomenon for AAMs derived from slowly reactive precursors. A similar behavior was observed for GP-rich AAM mortars, however, the mass loss was lower than the ISSA-rich specimens.

3.4 Change in mechanical properties

3.4.1 Compressive and flexural strength of AAMs

Figure 7 shows the compressive and flexural strength of AAM mortars after 6 months of water curing. It was observed that the compressive and flexural strength of the AAM samples increased as the amount of GP and GGBS increased, while it decreased as the amount of ISSA increased. Considering similar proportions of the ternary precursors, the specimens prepared with ISSA possessed low compressive strength (less than 10 MPa), and flexural strengths (less than 3 MPa). This behavior was due to the lower reactivity of the ISSA in a given alkaline environment compared to GGBS and GP. According to guidelines set by BS EN 1504 for repair materials, materials for structural repair class R4 must have a minimum compressive strength of 45 MPa or greater. The white line in the ternary diagram (in Fig. 7a) demarcates the specimens that met the required criteria. Based on the analysis, the optimum range for precursor materials with respect to GGBS, GP, and ISSA to produce class R4 repairing mortars, is 50–100%, 0–45%, and 0–25%, respectively. In addition, the maximum flexure strength development was observed in the ternary diagram shown in Fig. 8b, with almost similar ranges to the compressive strength one.

3.4.2 Flexural strength loss of AAMs after sewage corrosion

After the sewage corrosion test, changes in the fleural strength of the AAMs were measured. Two regions from Fig. 8 should be noticed, corresponding to the higher strength losses. One region occurred with 30–70% GP, 10–20% ISSA and 30–40% GGBS, which suffered flexural strength losses ranging from 31.3 to 47.9%. Another region occurred in the AAMs with less than 10–20% GP, 10% ISSA and 50–70% slag, where the flexural strength losses were more than 20%. Interestingly, when less than 20% ISSA was used, the flexural strength loss of the GGBS-rich AAMs was negative (above the white line), meaning the flexural strength slightly increased after exposure

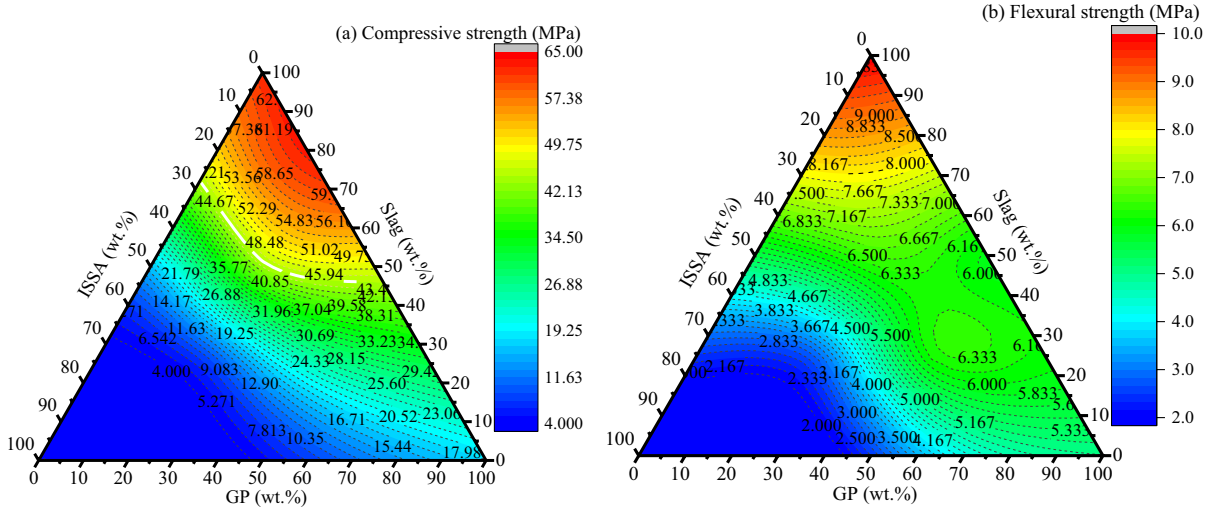

Fig.7 **a** Compressive strengths and **b**) flexural strength of the AAM mortars after 6 months of water curing

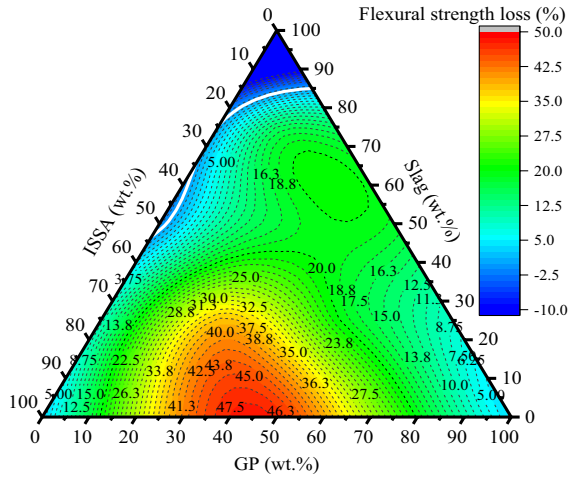

Fig. 8 Flexural strength loss of the AAM mortars after sewage corrosion

to the sewage environment. This enhancement effect in this region was ascribed to the optimal substitution level of the ISSA, which effectively controlled microbial growth and had a relatively high initial strength to counter erosion deterioration.

3.4.3 Compressive strength loss of AAMs after sewage corrosion

From Fig. 9a and b, an obvious difference is observed in compressive strength loss between the submerged and non-submerged areas, consistent with the phenomenon that corrosion of the sewer pipes was often not uniformly distributed. For the non-submerged area, the compressive strength loss appeared between the white lines, as shown in Fig. 9a. The submerged areas, however, all experienced compressive strength gains as shown in Fig. 9b. Considering the similar proportioning of the ternary precursors, the submerged area of the AAMs had a lower compressive strength loss than the non-submerged area. From Fig. 9a, the highest compressive strength loss in the non-submerged area was 20–35% when the 10–25% ISSA, 50–70% GP and 10–25% GGBS were used. For the submerged area (in Fig. 9b), the highest compressive strength gain was about 40% when the 10–15% ISSA, 50–60% GP and 10–20% GGBS were used. The results suggest that the non-submerged area of the AAMs was sensitive to the acid corrosion in the sewer, while the metabolism of SRB in the sewage solution has a weak effect on the strength development of non-submerged AAMs.

After the sewage corrosion test, the AAMs experienced a reduction in flexural and compressive strength due to acid corrosion, microbial corrosion, and physical erosion. The compressive strength loss of the non-submerged or submerged AAMs will be discussed later in the mineralogical and microstructural evolution section. Regardless of whether the AAMs were non-submerged or submerged, the compressive strength showed a slower loss than that of

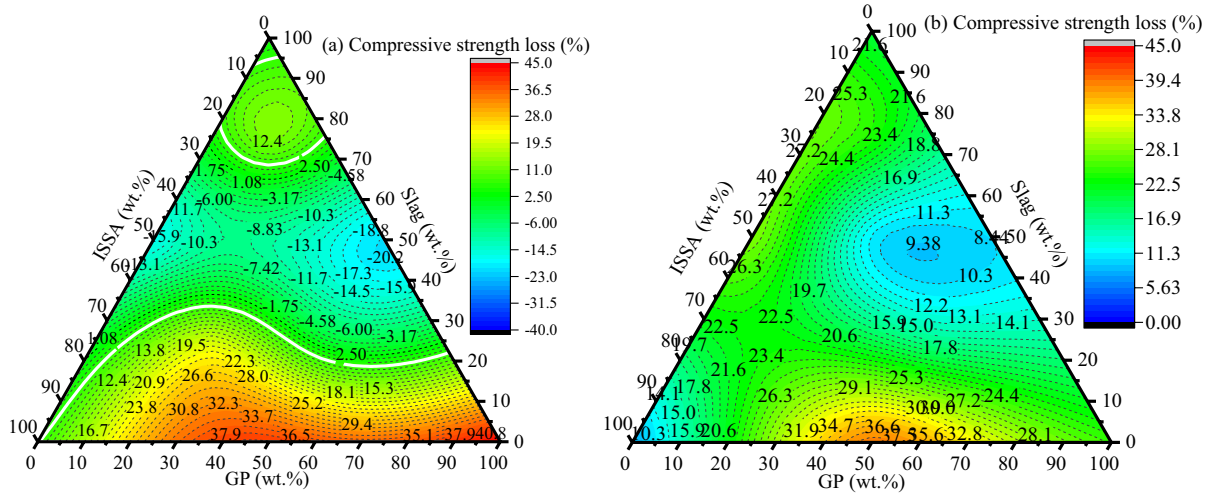

Fig. 9 Compressive strength loss of **a** non-submerged and **b** submerged area of AAMs exposed to sewage for 6 months

the flexural strength. The result illustrated that the most severe corrosion occurred in the area of AAMs at the sewage water mark level, followed by the non-submerged area, and the submerged area. The most serious deterioration occurred near the sewage water mark level was due to at this level sufficient water, nutrients and air were available for the growth of the microorganisms. Moreover, the corrosion of the AAM at the sewage water mark level was complex due to the fluctuation of wastewater levels and the hydraulic scouring effects, which accelerated the formation of microcracks. Therefore, at this level, there was a succession of microbial organism in the surface of AAMs. The coexistence of SOB and other bacteria was likely to appear near the sewage level mark of AAMs [40], which might lead to the formation of black biofilm in middle area of sample surface (as shown in Fig. 4). In addition, combined with the biofilm formation as shown in Fig. 4, the faint yellow or white biofilm formed on the non-submerged area of the AAM mortar, corresponding to the lower strength loss or growth. Therefore, it could be inferred that the faint yellow or white biofilm in the non-submerged area had a slightly protective effect on the AAM mortar to minimize the strength loss. In contrast, the black biofilm near the sewage level accelerated the corrosion of the AAMs by altering the transportation of oxygen and other chemicals involved in microbial metabolism, subsequently leading to a significant loss in flexural strength [41].

3.5 SEM/EDS

Figure 10 shows the SEM micrographs of the AAMs showing the morphological variations between the core and corrosion areas. To better understand the effect of GP and ISSA on the microstructural analysis of AAC mortars, those samples that contain high amount of ISSA or GP, were chosen. The core area of all AAMs showed the presence of amorphous gels, while the AAMs showed a loose and porous structure when more than 50% ISSA was added. Moreover, although gels were formed in the alkali-activated slag, some microcracks in the core area were related to the higher drying shrinkage [23]. In addition, after exposure to sewage for 6 months, the corrosion surface of AAMs contained some gypsum crystals since its formation at a low pH environment is preferred. The grain size of the gypsum crystals in the alkali-activated slag varied between 20 and 45 μm, while the grain size of gypsum in the AAMs with 25% ISSA decreased to less than 10 μm. This was consistent with the XRD results. For the alkali-activated slag, some microcracks were found due

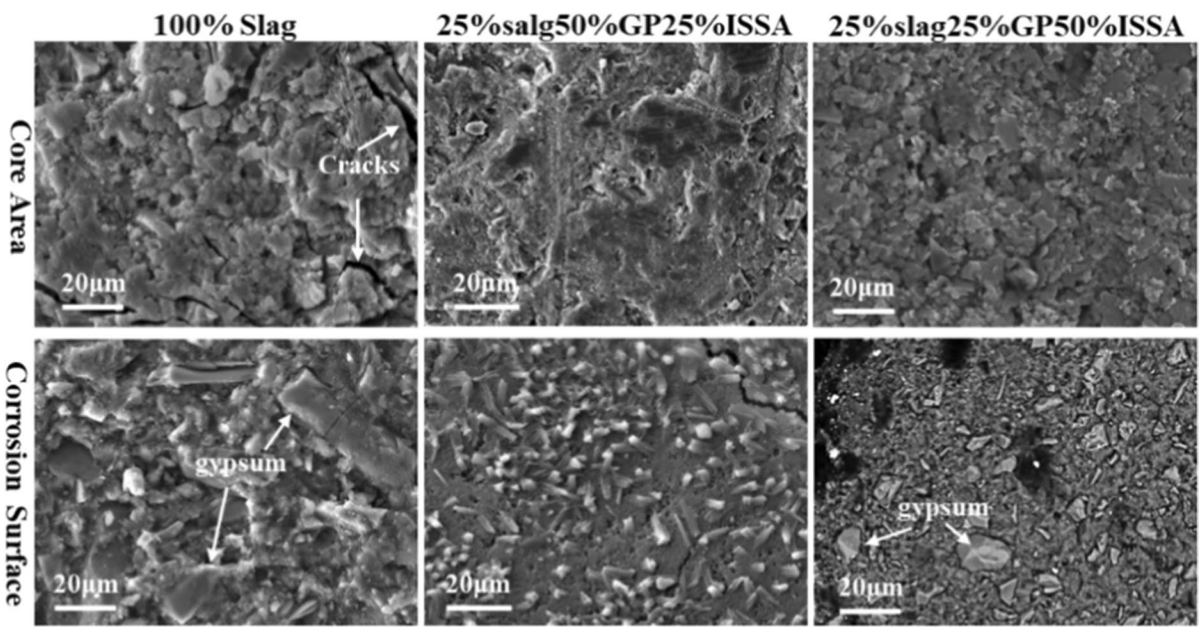

Fig. 10 Core and corrosion areas of AAMs exposed to sewage for 6 months

to the expansion caused by gypsum. Therefore, the formation of gypsum with a small grain size in AAMs with a rich ISSA content showed only slight expansion deterioration.

The element distributions of the AAMs exposed to sewage for 6 months were tested, and the line scan from the corrosion surface to the core area is shown in Fig. 11. Major elements, including Ca, Si, Al, O and Na, were found in all AAMs, implying the coexistence of C(–A)–S–H or C(–N)–A–S–H gels [42]. The line scans on the corrosion surface showed the concentrations of Ca in the AAMs decreased, indicating that the decalcification of the gels occurred significantly on the surface. Moreover, the Na concentrations were reduced in the corrosion surface due to the leaching of Na ions, especially for the alkali-activated slag. Furthermore, the concentrations of Ca, Si, Al, O and Na in the AAMs prepared with 50% ISSA were stable across the line scan. This might be due to the low gel content due to the low reactivity of ISSA. Besides, the concentration of S in all samples gradually increased from the core area to the corrosion surface, illustrating that the corrosion damage induced by the sulphate ions resulted from its diffusion from the outer sewage solution to the inner core region.

4 Discussion

4.1 Corrosion mechanism of sewage

As shown in Figs. 8, 9, the compressive strength loss of submerged and non-submerged areas showed an obvious difference, which was primarily attributed to the different deterioration mechanisms of microbial activity and acid erosion on the AAMs. In the sewage solution, the initial sulfate ions deposited in the sewage under the anaerobic environment were reduced by the sulfate-reducing bacteria (SRB) to form the hydrogen sulfide gas. To better evaluate the effect of metabolite on the corrosion mechanism of AAM, some samples were chosen for XRD analysis. From Fig. 12, a broad hump in the alkali-activated GGBS/GP (in the submerged areas) was detected at 25–35°, corresponding to a low crystallinity amorphous N–A–S–H/C(–A)–S–H gel. However, the AAMs with the ISSA contained crystalline phases, as shown in

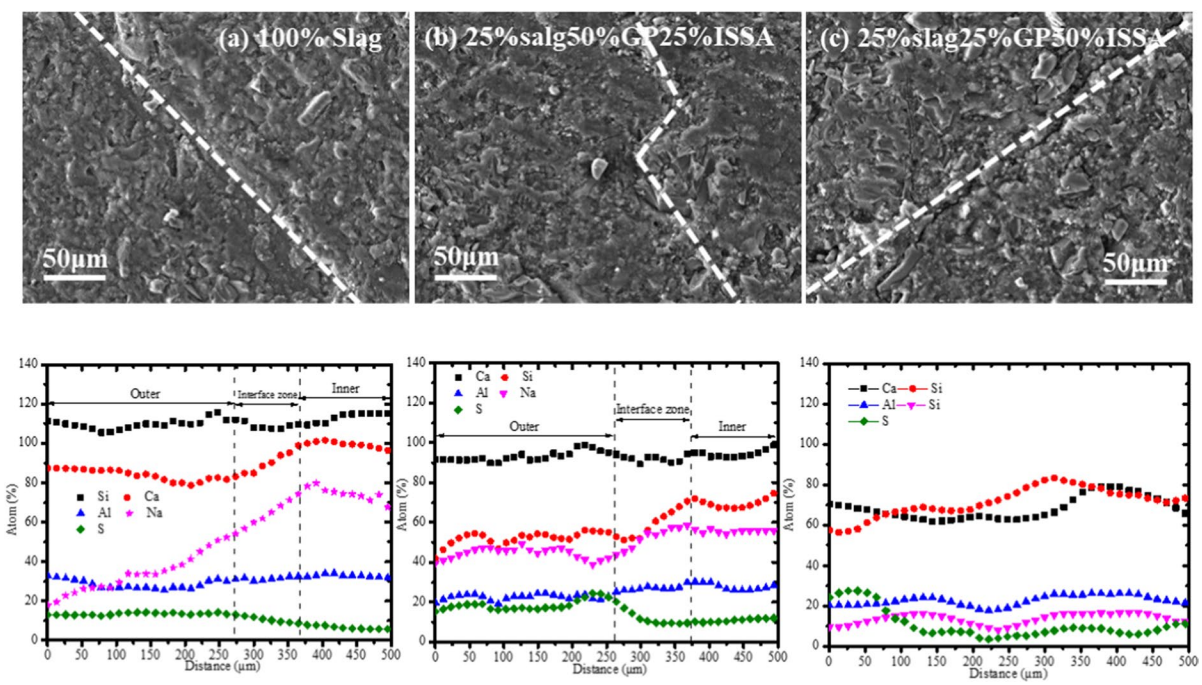

Fig. 11 SEM/EDS of the interfacial transition zone of AAMs between the core area and corrosion surface exposed to sewage for 6 months

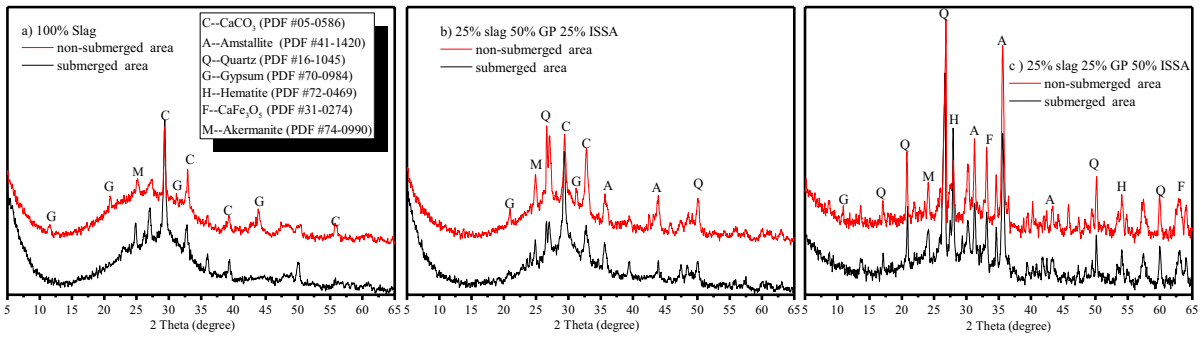

Fig. 12 XRD patterns of non-submerged and submerged areas of the AAMs after exposed to sewage for 6 months

Fig. 12b and c. These crystalline phases (e.g., quartz, hematite and CaFe3O5) were similar to those in the ISSA, so the presence of these minerals implied strong stability and low reactivity of the ISSA in the strong alkali solutions. After sewage corrosion, the reaction products of the submerged AAMs make no change, and so the sulfur-containing products from the SOB metabolism appeared to have a negligible effect on the properties of the AAM specimens. Therefore, for the submerged area of the AAMs, a small amount of microbial attachment and metabolism were identified as a major cause of deterioration, mainly occurring due to the interaction between the AAMs' surface and biofilm [6, 43]. However, this deterioration caused by the microbial attachment and metabolism appeared to be minimal for the submerged area of AAMs.

For the non-submerged area, hydrogen sulfide gas escaped from the sewage to the upper unfilled space and was oxidized to sulfuric acid by the sulfur-oxidizing bacteria (SOB) under aerobic conditions [4, 6]. Deterioration is caused by acid excretion which etches the surface of concrete, penetrating the AAMs mortar surface, especially in sewer systems. Therefore, the deterioration mechanism of the non-submerged area was a dominantly biogenic sulfuric acid attack, and was due to the decomposition of products (dealumination and decalcification/desodiumization of N–(C)–A–S–H and C–A–S–H gels) [44, 45]. It should be noted that migration of acid-containing condensates from the upper part (non-submerged part) of the samples triggered the high corrosion rates around the waterline. From Fig. 12, the non-submerged area of the AAMs showed diffraction peaks of gypsum, illustrating that the biogenic sulfuric acid induced the decomposition of the gels. Moreover, the absence of sulphoaluminate phases in the AAMs after the sewage corrosion illustrated that the formed gypsum did not further react with the aluminate phases. Overall, one important consequence related to the formation of gypsum may be the volume expansion which may ultimately lead to the deterioration of the AAMs in non-submerged areas. But the reasons for the superior performance of the GP/GGBS-rich AAMs (between the white lines) were attributed to the acid buffering capacity of the aluminum phase and the formation of a pore-filling aluminum gel that exhibited better cohesion to the degraded layer, as discussed in previous [46–48].

4.2 Inhibition mechanism of ISSA

Over the last few years, antimicrobial agents that had been reported to be applied in the construction sector included heavy metals (nickel, tungsten), and metal compounds (silver molybdate, copper oxide, zinc oxide,), but the use of these agents in the construction sector was very limited since the environmental concern. To understand the effect of the heavy metals from ISSA on microbial activity, the leaching characteristic from the AAMs with and without the ISSA was evaluated by the ASTM C1308, and the results are shown in Fig. 13. For all AAMs, the concentrations of leached metals were below the stipulated TCLP (toxicity characteristic leaching procedure) limits, so these AAMs could be considered safe and pose little detrimental effects to the environment. However, the leached heavy metal (e.g., Zn, Cu, Co and Pb) could inhibit the life-essential activity of sensitive enzymes and disturb the osmotic stability of the

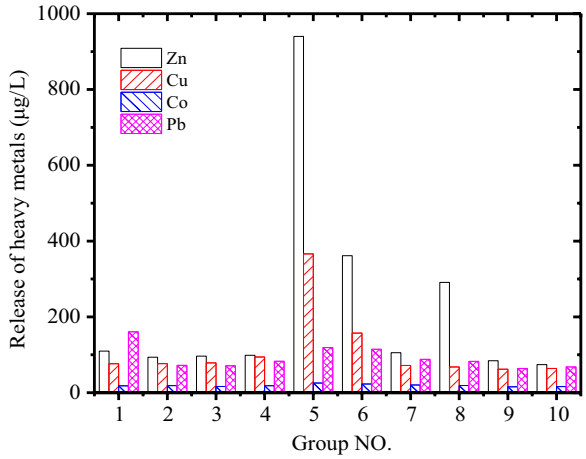

Fig. 13 Leaching concentrations of the AAMs

Table 3 The average crystal size of gypsum in the AAMs

	Crystal face		Average crystal size (Å)
	(020)	(−121)	
100% slag	391	335	379.5
25% GGBS 50% GP 25% ISSA	378	330	354
25% GGBS 25% GP 50% ISSA	283	291	287

cell of bacteria, resulting in the leakage of intracellular constituents [49–51]. Relatively higher concentrations of Zn and Cu could be found in the AAMs (samples 5, 6 and 8) when more than 50% ISSA was added. As shown in Figs. 6, 7, 8, these AAMs showed the lowest mass loss and strength loss. Moreover, little biofilm could be seen in the non-submerged area for samples 5, 6, 7 and 8 as depicted in Fig. 4, illustrating the antimicrobial effect of ISSA due to the heavy metals leaching.

The expansion damage of gypsum in cementitious was generally related to its crystal size, and a high crystal size would cause obvious expansion damage. According to the Scherrer formulae [52], the crystal size of gypsum in the non-submerged area could be calculated. From Table 3, the crystal size of gypsum in (0 2 0) and (−1 2 1) faces decreased with the increase of ISSA content, implying the formation of gypsum with a smaller size leading to smaller expansion. The result could be also observed by SEM of corrosion areas of AAMs (in Fig. 10). The reason was attributed to the fact replacing GGBS with ISSA decreased the calcium content. As a result, the available calcium could be a significant source for the formation of gypsum grain. Although the formation of large-sized gypsum grain, the GGBS-rich AAMs showed a lower level of strength deterioration (as shown in Figs. 8 and 9). This reason can be attributed to the larger size gypsum crystals that seemed to help form a compact core–shell structure on the surface of the AAMs. This thick nodular gypsum layer on the surface might reduce the deterioration and diffusion of ions, and this finding was consistent with our previous study on the sulfuric acid attack of AAMs [48]. Overall, the improvement effect of ISSA on the sewage erosion of the AAMs resulted from the heavy metals as antimicrobial agents, and the low calcium content.

5 Conclusions

The durability of AAM mortar subjected to sewage-aggressive environments was investigated, and the main conclusions can be summarized as follows:

(1) The AAMs mortar exposure to sewage aggressive environments showed significant mass and strength losses. The highest mass loss was about 18%, and the highest flexural and compressive strength losses could reach 50% and 40%, respectively.
(2) The incorporation of the ISSA reduced the compressive and flexural strength of the AAM mortar. But the AAMs prepared with a low substitution level of ISSA effectively controlled microbial

growth. This improved behavior induced by the ISSA was attributed to their gel matrices with relatively low available Ca, which reduced the decalcification and grain size of gypsum (and the expansive deterioration). Moreover, the leaching of heavy metals from the ISSA had a bacteriostatic effect on the bacterial activities, which decreased the bioerosion.

(3) The most severe deterioration of AAMs occurred near the water level of the sewage due to microbial metabolism, and the smallest deterioration occurred in the submerged area. The deterioration that occurred in the non-submerged area was due to the presence of biogenic sulfuric acid. However, the formation of biofilms in the non-submerged area to some extent had some protective effect on the AAMs.

(4) Although the concentrations of leached heavy metals from the AAMs with the ISSA were below the stipulated TCLP limits, the slight leaching of the heavy metal (e.g., Zn, Cu, Co and Pb) as a bactericide could inhibit the formation of biofilm and microbial metabolism.

The study investigated the potential use of ISSA as a source of bactericidal agent in the AAMs to enhance sewer rehabilitation. The leaching of heavy metal (e.g., Zn, Cu, Co and Pb) from the ISSA could inhibit the microbial metabolism and enhance the durability of AAMs exposed to the sewage, but the challenges arise, particularly for the most severe corrosion near the sewage level. To overcome these issues, further research is recommended, including the exploration of heavy metals-gradient modified AAMs. Additionally, the exploration of bacterial communities using various advanced mineral analytical techniques (e.g., 16S rRNA gene amplicon sequencing) could be considered, potentially elucidating the erosion mechanism of the microorganism on the AAMs. Ongoing research is essential to address these issues and verify the proposed method for a more sustainable AAMs application.

Acknowledgements This study work was supported by a Grant from the Research Grants Council (NO. P0033406 & B-Q80K) and The Hong Kong Polytechnic University.

Author contributions Keke Sun: Conceptualization, Methodology, Visualization, Writing—original draft, Writing-review & editing. Hafiz Asad Ali: Conceptualization, Visualization, Writing—review & editing. Yamei Cai and Dongxing Xuan: Supervision and Writing—review & editing. Chi Sun Poon: Conceptualization, Resources, Project administration, Supervision.

Funding Open access funding provided by The Hong Kong Polytechnic University.

Declarations

Conflict of interest The authors declare that they have no known competing financial interests or personal relationships that could have appeared to influence the work reported in this paper.

References

1. Wu L, Huang G, Liu W (2021) Methods to evaluate resistance of cement-based materials against microbially induced corrosion: a state-of-the-art review. Cem Concr Compos 123:104208. https://doi.org/10.1016/j.cemconcomp.2021.104208
2. Islander R, Devinny J, Mansfeld F, Postyn A, Shih H (1991) Microbial ecology of crown corrosion in sewers. J Env Eng 117(6):751–770. https://doi.org/10.1061/(ASCE)0733-9372(1991)117:6(751)
3. Rong H, Zhang S, Ma G, Zheng X, Qian C, Zhang L, Zhang Y, Xu R (2021) Formation, growth and corrosion effect of sulfur oxidizing bacteria biofilm on mortar. Constr Build Mater 268(25):121218. https://doi.org/10.1016/j.conbuildmat.2020.121218
4. Mori T, Tazaki K (1992) Interactions of nutrients, moisture and pH on microbial corrosion of concrete sewer pipes. Water Res 26(1):29–37. https://doi.org/10.1016/0043-1354(92)90107-F
5. Grengg C, Mittermayr F, Ukrainczyk N, Koraimann G, Kienesberger S, Dietzel M (2018) Advances in concrete materials for sewer systems affected by microbial induced concrete corrosion: a review. Water Res 134:341–352. https://doi.org/10.1016/j.watres.2018.01.043
6. O'Connell M, McNally C, Richardson M (2010) Biochemical attack on concrete in wastewater applications: a

state of the art review. Cem Concr Compos 32:479–485. https://doi.org/10.1016/j.cemconcomp.2010.05.001
7. Alexander M, Fourie C (2011) Performance of sewer pipe concrete mixtures with portland and calcium aluminate cements subject to mineral and biogenic acid attack. Mater Struct 44:313–330. https://doi.org/10.1617/s11527-010-9629-1
8. Kong L, Fang J, Zhou X, Han M, Lu H (2018) Assessment of coatings for protection of cement paste against microbial induced deterioration through image analysis. Constr Build Mater 191:342–353. https://doi.org/10.1016/j.conbuildmat.2018.10.041
9. Soleimani S, Ormeci B, Isgor OB (2013) Evaluation of E. coli biofilm as a protective barrier against microbiologically influenced deterioration of concrete (MICD) under mesophilic temperatures. Water Sci Technol 68:303–310. https://doi.org/10.2166/wst.2013.252
10. Scarfato P, Di Maio L, Fariello M, Russo P, Incarnato L (2012) Preparation and evaluation of polymer/clay nanocomposite surface treatments for concrete durability enhancement. Cem Concr Compos 34:297–305. https://doi.org/10.1016/j.cemconcomp.2011.11.006
11. Bu C, Wen K, Liu S, Ubani O, Lin L (2018) Development of bio-cemented constructional materials through microbial induced calcite precipitation. Mater Struct 51:1–11. https://doi.org/10.1617/s11527-018-1157-4
12. Kong L, Zhao W, Xuan D, Wang X, Liu Y (2022) Application potential of alkali-activated concrete for antimicrobial induced corrosion: A review. Constr Build Mater 317(24):126169. https://doi.org/10.1016/j.conbuildmat.2021.126169
13. Zhang J, Shi C, Zhang Z, Ou Z (2017) Durability of alkali-activated materials in aggressive environments: A review on recent studies. Constr Build Mater 152(15):598–613. https://doi.org/10.1016/j.conbuildmat.2017.07.027
14. Grengg C, Gluth G, Mittermayr F (2023) Alkali-activated materials for sewers. Microbiologically influenced corrosion of concrete sewers: mechanisms, measurements, modelling and control strategies. Springer International Publishing, Cham, pp 233–247
15. Gu J, Ford T, Mitchell R (2011) Microbiological corrosion of concrete. Uhlig's corrosion handbook. Wiley, New Jersey, pp 477–491
16. Provis J, Palomo A, Shi C (2015) Advances in understanding alkali-activated materials. Cem Concr Res 78:110–125. https://doi.org/10.1016/j.cemconres.2015.04.013
17. Provis J (2009) Activating solution chemistry for geopolymers. Geopolymers: structures processing properties and industrial applications. Woodhead Publishing, Cambridge, pp 50–71
18. Sun K, Peng X, Wang S, Zeng L (2019) Design method for the mix proportion of geopolymer concrete based on the paste thickness of coated aggregate. J Clean Prod 232(20):508–517. https://doi.org/10.1016/j.jclepro.2019.05.254
19. Ling T, Poon C, Wong H (2013) Management and recycling of waste glass in concrete products: current situations in Hong Kong. Resour Conserv Recycl 70:25–31. https://doi.org/10.1016/j.resconrec.2012.10.006
20. Redden R, Neithalath N (2014) Microstructure, strength, and moisture stability of alkali activated glass powder-based binders. Cem Concr Compos 45:46–56. https://doi.org/10.1016/j.cemconcomp.2013.09.011
21. Swann L, Downs D, Waye M (2017) Waste to energy solution-the sludge treatment facility in Tuen Mun, Hong Kong. Energy Procedia 143:500–505. https://doi.org/10.1016/j.egypro.2017.12.717
22. Li J, Xue Q, Fang L, Poon C (2017) Characteristics and metal leachability of incinerated sewage sludge ash and air pollution control residues from Hong Kong evaluated by different methods. Waste Manag 64:161–170. https://doi.org/10.1016/j.wasman.2017.03.033
23. Sun K, Ali H, Xuan D, Ban J, Poon C (2022) Utilization of APC residues from sewage sludge incineration process as activator of alkali-activated slag/glass powder material. Cem Concr Compos 133:104680. https://doi.org/10.1016/j.cemconcomp.2022.104680
24. Sun K, Ali H, Ji W, Ban J, Poon C (2023) Utilization of contaminated air pollution control residues generated from sewage sludge incinerator for the preparation of alkali-activated materials. Resour Conserv Recycl 188:106665. https://doi.org/10.1016/j.resconrec.2022.106665
25. Chen Z, Li J, Zhan B, Sharma U, Poon C (2018) Compressive strength and microstructural properties of dry-mixed geopolymer pastes synthesized from GGBS and sewage sludge ash. Constr Build Mater 182(10):597–607. https://doi.org/10.1016/j.conbuildmat.2018.06.159
26. Yio M, Phelan J, Wong H, Buenfeld N (2014) Determining the slag fraction, water/binder ratio and degree of hydration in hardened cement pastes. Cem Conc Res 56:171–181. https://doi.org/10.1016/j.cemconres.2013.12.002
27. Li M, Yao J, Sunahara G, Hawari J, Duran R, Liu J, Liu B, Cao Y, Ruan Z (2022) Novel microbial consortia facilitate metalliferous immobilization in non-ferrous metal(loid)s contaminated smelter soil: Efficiency and mechanisms. Environ Pollut 313(15):120042. https://doi.org/10.1016/j.envpol.2022.120042
28. Khan H, Yasir M, Castel A (2022) Performance of cementitious and alkali-activated mortars exposed to laboratory simulated microbially induced corrosion test. Cem Concr Compos 128:104445. https://doi.org/10.1016/j.cemconcomp.2022.104445
29. Moloantoa K, Khetsha Z, Mochane M, Unuofin J, Atangana A, Cason E, van Heerden E, Castillo J (2023) Evaluating the effects of pH and temperature on sulphate-reducing bacteria and modelling of their effects in stirred bioreactors. Environ Pollut Bioavail 35:2257388. https://doi.org/10.1080/26395940.2023.2257388
30. APH (2012) Standard methods for the examination of water and wastewater. American Public Health Association.
31. Hoštacká A, Čižnár I, Štefkovičová M (2010) Temperature and pH affect the production of bacterial biofilm. Folia Microbiol 55:75–78. https://doi.org/10.1007/s12223-010-0012-y
32. Else T, Pantle C, Amy P (2003) Boundaries for biofilm formation: humidity and temperature. Appl and Environ Microb 69:5006–5010

33. Visvanathan C, Aim RB, Parameshwaran K (2000) Membrane separation bioreactors for wastewater treatment. Crit Rev Environ Sci Technol 30:1–48. https://doi.org/10.1128/AEM.69.8.5006-5010.2003
34. Kong L, Liu C, Cao M, Fang J (2018) Mechanism study of the role of biofilm played in sewage corrosion of mortar. Constr Build Mater 164(10):44–56. https://doi.org/10.1016/j.conbuildmat.2017.12.190
35. W Wu M, Wang T and Wang S (2020) Corrosion and sulfur-related bacteria. In: Environmental technologies to treat sulfur pollution: principles and engineering
36. O'Toole G, Kaplan H, Kolter R (2000) Biofilm formation as microbial development. Annu Rev Microbiol 54(1):49–79. https://doi.org/10.1146/annurev.micro.54.1.49
37. Khan H, Castel A, Khan M (2020) Corrosion investigation of fly ash based geopolymer mortar in natural sewer environment and sulphuric acid solution. Corros Sci 168(15):108586. https://doi.org/10.1016/j.corsci.2020.108586
38. Fernandes I, Pericão M, Hagelia P, Noronha F, Ribeiro M, Maia J (2012) Identification of acid attack on concrete of a sewage system. Mater Struct 45:337–350. https://doi.org/10.1617/s11527-011-9769-y
39. Dhami N, Reddy S, Mukherjee A (2012) Biofilm and microbial applications in biomineralized concrete. Adv Top Biominer 2:137–164
40. Song Y, Tian Y, Li X, Wei J, Zhang H, Bond P, Yuan Z, Jiang G (2019) Distinct microbially induced concrete corrosion at the tidal region of reinforced concrete sewers. Water Res 150:392–402. https://doi.org/10.1016/j.watres.2018.11.083
41. Simoes L, Simoes M, Vieira M (2010) Influence of the diversity of bacterial isolates from drinking water on resistance of biofilms to disinfection. App Env Microbiol 76(2):6673–6679. https://doi.org/10.1128/AEM.00872-10
42. Walkley B, San Nicolas R, Sani M, Rees G, Hanna J, van Deventer J, Provis J (2016) Phase evolution of C-(N)-ASH/NASH gel blends investigated via alkali-activation of synthetic calcium aluminosilicate precursors. Cem Concr Res 89:120–135. https://doi.org/10.1016/j.cemconres.2016.08.010
43. Roychand R, Li J, De Silva S, Saberian M, Law D, Pramanik B (2021) Development of zero cement composite for the protection of concrete sewage pipes from corrosion and fatbergs. Resour Conserv Recycl 164:105166. https://doi.org/10.1016/j.resconrec.2020.105166
44. Ye H, Huang L (2020) Degradation mechanisms of alkali-activated binders in sulfuric acid: the role of calcium and aluminum availability. Constr Build Mater 246(20):118477. https://doi.org/10.1016/j.conbuildmat.2020.118477
45. Wang Y, Cao Y, Zhang Z, Zhang P, Ma Y, Wang A, Wang H (2023) Intrinsic sulfuric acid resistance of C-(N)-A-S-H and N-A-S-H gels produced by alkali-activation of synthetic calcium aluminosilicate precursors. Cem Concr Res 165:107068. https://doi.org/10.1016/j.cemconres.2022.107068
46. Herisson J, Gueguen-Minerbe M, van Hullebusch E, Chaussadent T (2017) Influence of the binder on the behaviour of mortars exposed to H2S in sewer networks: a long-term durability study. Mater Struct 50(8):1–18. https://doi.org/10.1617/s11527-016-0919-0
47. Grengg C, Ukrainczyk N, Koraimann G, Mueller B, Dietzel M, Mittermayr F (2020) Long-term in situ performance of geopolymer, calcium aluminate and Portland cement-based materials exposed to microbially induced acid corrosion. Cem Concr Res 131:106034. https://doi.org/10.1016/j.cemconres.2020.106034
48. Sun K, Ali H, Xuan D, Poon C (2024) Sulfuric acid resistance behaviour of alkali-activated slag and waste glass powder blended precursors. Cem Concr Compos 145:105319. https://doi.org/10.1016/j.cemconcomp.2023.105319
49. Kong L, Zhang B, Fang J (2018) Effect of bactericide on the deterioration of concrete against sewage. J Mater Civ Eng 30:04018160. https://doi.org/10.1061/(ASCE)MT.1943-5533.0002358
50. Haile T, Nakhla G, Allouche E, Vaidya S (2010) Evaluation of the bactericidal characteristics of nano-copper oxide or functionalized zeolite coating for bio-corrosion control in concrete sewer pipes. Corros Sci 52(1):45–53. https://doi.org/10.1016/j.corsci.2009.08.046
51. Qiu L, Dong S, Ashour A, Han B (2020) Antimicrobial concrete for smart and durable infrastructures: a review. Constr Build Mater 260(10):120456. https://doi.org/10.1016/j.conbuildmat.2020.120456
52. Patterson A (1939) The Scherrer formula for X-ray particle size determination. Phys Rev 56(10):978–982. https://doi.org/10.1103/PhysRev.56.978